A Mutually Exciting Latent Space Hawkes Process Model for Continuous-time Networks (Supplementary material)

Zhipeng Huang[1] **Hadeel Soliman**[1] **Subhadeep Paul**[2] **Kevin S. Xu**[1]

[1]Department of Electrical Engineering and Computer Science, University of Toledo, Toledo, OH, USA
[2]Department of Statistics, The Ohio State University, Columbus, OH, USA

Abstract

Networks and temporal point processes serve as fundamental building blocks for modeling complex dynamic relational data in various domains. We propose the *latent space Hawkes (LSH)* model, a novel generative model for continuous-time networks of relational events, using a latent space representation for nodes. We model relational events between nodes using mutually exciting Hawkes processes with baseline intensities dependent upon the distances between the nodes in the latent space and sender and receiver specific effects. We demonstrate that our proposed LSH model can replicate many features observed in real temporal networks including reciprocity and transitivity, while also achieving superior prediction accuracy and providing more interpretable fits than existing models.

A ADDITIONAL MODEL AND ESTIMATION DETAILS

A.1 PROOF OF THEOREM 3.1

Proof. Suppose two sets of parameters $\theta_2, Z, \gamma, \delta$ and $\theta_2', Z', \gamma', \delta'$ lead to the same $\log(\mu)$:

$$\theta_2 J_n + ZZ^T + \tilde{\delta}1_n^T + 1_n\tilde{\gamma}^T = \theta_2' J_n + Z'Z'^T + \tilde{\delta}'1_n^T + 1_n\tilde{\gamma}'^T.$$

Left multiplying both sides by 1_n^T and noting that (i) $1_n^T Z = 1_n^T HZ = 1_n^T(I_n - \frac{1}{n}1_n 1_n^T)Z = 0$ by assumption 1 and (ii) $1_n^T\tilde{\delta} = 0$ by assumption 2, we get

$$\begin{aligned} &1_n^T\theta_2 J_n + 1_n^T 1_n\tilde{\gamma}^T = 1_n^T\theta_2' J_n + 1_n^T 1_n\tilde{\gamma}'^T \\ &\Rightarrow n(\theta_2 - \theta_2')1_n^T + n(\tilde{\gamma}^T - \tilde{\gamma}'^T) = 0 \end{aligned} \tag{A.1}$$

Now, right multiplying by 1_n we get

$$n^2(\theta_2 - \theta_2') = 0$$

because $\gamma^T 1_n = 0$ and $\tilde{\gamma}^T 1_n = 0$ by our identifiability constraints. This implies that $\theta_2 = \theta_2'$. With this, using A.1, we have

$$n(\tilde{\gamma}^T - \tilde{\gamma}'^T) = 0 \Rightarrow \tilde{\gamma} = \tilde{\gamma}'.$$

Finally, right multiplying by 1_n from the beginning and then using the above result $\theta_2 = \theta_2'$ we have

$$\begin{aligned} &\theta_2 J_n 1_n + \tilde{\delta}1_n^T 1_n = \theta_2' J_n 1_n + \tilde{\delta}'1_n^T 1_n \\ &\Rightarrow n(\tilde{\delta} - \tilde{\delta}') = 0, \quad \Rightarrow \tilde{\delta} = \tilde{\delta}'. \end{aligned}$$

In light of the above results we then conclude

$$ZZ^T = Z'Z'^T.$$

Accepted for the 38th Conference on Uncertainty in Artificial Intelligence (UAI 2022).

which means $Z = Z'O$ where $O_{d\times d}$ is an orthogonal matrix such that $OO^T = I$. Furthermore, from the results of Ozaki [1979], the baseline intensity μ_{uv} and jump size parameters α_1, α_2 are identified, i.e. if two sets of $\mu_{uv}, \alpha_1, \alpha_2$ lead to the same probability density function (log-likelihood), then the two sets must be identical. □

A.2 FULL LOG-LIKELIHOOD EXPRESSION

Let $\Lambda_{uv}(t_k^{uv}) = \int_0^{t_k} \lambda_{uv}^*(t)\,dt$. We can break the time interval $[0, t_k]$ to $[0, t_1], [t_1, t_2], \ldots, [t_{k-1}, t_k]$, resulting in

$$
\begin{aligned}
\Lambda_{uv}(t_k^{uv}) &= \int_0^{t_k^{uv}} \lambda_{uv}^*(t)\,dt \\
&= \int_0^{t_1^{uv}} \lambda_{uv}^*(t)\,dt + \sum_{i=1}^{k-1} \int_{t_i^{uv}}^{t_{i+1}^{uv}} \lambda_{uv}^*(t)\,dt \\
&= \int_0^{t_1^{uv}} \mu_{uv}\,dt + \sum_{i=1}^{k-1} \int_{t_i^{uv}}^{t_{i+1}^{uv}} \left[\mu_{uv} + \sum_{j:t_j^{uv}<t_i^{uv}} \sum_b^B C_b\alpha_1\beta_b e^{-\beta_b(t-t_j^{uv})} + \sum_{j:t_j^{vu}<t_i^{uv}} \sum_b^B C_b\alpha_2\beta_b e^{-\beta_b(t-t_j^{vu})}\right] dt \\
&= \mu_{uv}t_k^{uv} + \sum_{i=1}^{k-1} \int_{t_i^{uv}}^{t_{i+1}^{uv}} \sum_b^B \left[\sum_{j:t_j^{uv}<t_i^{uv}} C_b\alpha_1\beta_b e^{-\beta_b(t-t_j^{uv})} + \sum_{j:t_j^{vu}<t_i^{uv}} C_b\alpha_2\beta_b e^{-\beta_b(t-t_j^{vu})}\right] dt \\
&= \mu_{uv}t_k^{uv} + \sum_{i=1}^{k-1} \sum_{j:t_j^{uv}<t_i^{uv}} \sum_b^B \int_{t_i^{uv}}^{t_{i+1}^{uv}} \left[C_b\alpha_1\beta_b e^{-\beta_b(t-t_j^{uv})}\right] dt + \sum_{i=1}^{k-1} \sum_{j:t_j^{vu}<t_i^{uv}} \sum_b^B \int_{t_i^{uv}}^{t_{i+1}^{uv}} \left[C_b\alpha_2\beta_b e^{-\beta_b(t-t_j^{vu})}\right] dt \\
&= \mu_{uv}t_k^{uv} - \sum_{i=1}^{k-1} \sum_b^B \sum_{j:t_j^{uv}<t_i^{uv}} C_b\alpha_1 \left[e^{-\beta_b(t_{i+1}^{uv}-t_j^{uv})} - e^{-\beta_b(t_i^{uv}-t_j^{uv})}\right] \\
&\qquad - \sum_{i=1}^{k-1} \sum_b^B \sum_{j:t_j^{vu}<t_i^{uv}} C_b\alpha_2 \left[e^{-\beta_b(t_{i+1}^{uv}-t_j^{vu})} - e^{-\beta_b(t_i^{uv}-t_j^{vu})}\right]
\end{aligned}
\tag{A.2}
$$

By extending the summation, many of terms can cancel out, and then we can simplify $\Lambda_{uv}(t_k^{uv})$ as follows:

$$
\Lambda_{uv}(t_k^{uv}) = \mu_{uv}t_k^{uv} - \sum_b^B C_b\alpha_1 \sum_{j:t_j^{uv}<t_k^{uv}} \left[e^{-\beta_b(t_k^{uv}-t_j^{uv})} - 1\right] - \sum_b^B C_b\alpha_2 \sum_{j:t_j^{vu}<t_k^{uv}} \left[e^{-\beta_b(t_k^{uv}-t_j^{vu})} - 1\right]. \tag{A.3}
$$

Substituting (A.3) into (5) gives the following simplified expression for the log-likelihood.

$$
\begin{aligned}
l = \sum_{u\neq v} \Bigg\{ &\sum_{i=1}^{k} \log \left[\mu_{uv} + \sum_{j:t_j^{uv}<t_i^{uv}} \sum_b^B C_b\alpha_1\beta_b e^{-\beta_b(t_i^{uv}-t_j^{uv})} + \sum_{j:t_j^{vu}<t_i^{uv}} \sum_b^B C_b\alpha_2\beta_b e^{-\beta_b(t_i^{uv}-t_j^{vu})}\right] \\
&- \mu_{uv}t_k^{uv} + \sum_b^B C_b\alpha_1 \sum_{j:t_j^{uv}<t_k^{uv}} \left[e^{-\beta_b(t_k^{uv}-t_j^{uv})} - 1\right] - \sum_b^B C_b\alpha_2 \sum_{j:t_j^{vu}<t_k^{uv}} \left[e^{-\beta_b(t_k^{uv}-t_j^{vu})} - 1\right] \Bigg\}.
\end{aligned}
\tag{A.4}
$$

We use the negative of the log-likelihood expression in (A.4) as the objective function for the L-BFGS-B minimization.

A.3 ALTERNATING MINIMIZATION

An alternative approach to obtaining the maximum likelihood estimate (MLE) is to partition our parameters into two sets: the latent node positions Z and all other parameters $\Theta = (\alpha_1, \alpha_2, \theta_1, \theta_2, \delta, \gamma)$. We propose an alternating minimization approach to obtain the MLE. It alternates between optimizing the NLL over the estimated latent positions $\hat{Z}$ while holding all other parameters fixed and optimizing all other parameters $\hat{\Theta}$ while holding the latent positions fixed.

Algorithm A.1 Alternating minimization estimation algorithm

Input: Relational event triplets (u, v, t), latent dimension d, kernel decays β, kernel scale parameters C
Initialize $\hat{Z}$ using multidimensional scaling
Initialize $\hat{\Theta}$ randomly
repeat
  $\hat{\Theta} \leftarrow s_\theta$ steps of L-BFGS-B over $\hat{\Theta}$ on log-likelihood (A.4) while keeping $\hat{Z}$ fixed
  $\hat{Z} \leftarrow s_Z$ steps of L-BFGS-B over $\hat{Z}$ on log-likelihood (A.4) while keeping $\hat{\Theta}$ fixed
until log-likelihood (A.4) converges
Return: Estimated model parameters $(\hat{Z}, \hat{\Theta})$

Algorithm B.1 Generative procedure for Latent space Hawkes network

Input: Number of nodes n, time duration T, latent dimension d, kernel decays β, kernel scaling parameters C, model parameters $(\theta_1, \theta_2, \alpha_1, \alpha_2)$
Sample latent positions Z and sender and receiver effects δ, γ from Normal distributions: $Z \leftarrow \mathcal{N}(0, \sigma_z^2 I_{nd}), \delta \leftarrow \mathcal{N}(0, \sigma_\delta^2 I_n), \gamma \leftarrow \mathcal{N}(0, \sigma_\gamma^2 I_n)$
Set $Z \leftarrow Z\sqrt{|\theta_1|}, \theta_1 \leftarrow \theta_1/\sqrt{|\theta_1|}$ to remove identifiability issues
for all node pairs $u \neq v$ **do**
  $\mu_{uv} \leftarrow e^{-\theta_1 ||z_u - z_v||_2^2 + \theta_2 + \delta_u + \gamma_v}$
  $\mathcal{H}(u, v) \leftarrow$ Ogata's thinning algorithm $(\mu_{uv}, \alpha_1, \alpha_2, T, \beta, C)$
end for
Return: Simulated network $\mathcal{H}$ containing events $\mathcal{H}(u, v)$ for all $u \neq v$

We run each minimization over a fixed number of iterations and then switch to the other minimization. We experiment with different values for the number of steps (s_Θ, s_Z) denoting the number of iterations to run the optimization over Θ and Z, respectively. We find that there is not much difference in the performance for different numbers of steps for the directions in alternate minimization. Taking 2 steps in each directions, i.e. $s_\Theta = 2, s_Z = 2$, seems to work well. Pseudocode for our alternating minimization estimation procedure is shown in Algorithm A.1.

B ADDITIONAL EXPERIMENT RESULTS

B.1 SIMULATED NETWORKS

The generative process for the simulated networks is shown in Algorithm B.1. As discussed in Theorem 3.1, the latent positions Z are only identifiable up to a rotation. Furthermore, the slope parameter θ_1 is not identifiable, so we absorb it into the latent positions by setting

$$\hat{Z} \leftarrow \hat{Z}\sqrt{|\hat{\theta}_1|} \qquad \text{and} \qquad \hat{\theta}_1 \leftarrow \frac{\hat{\theta}_1}{\sqrt{|\hat{\theta}_1|}}.$$

Then, to compare the estimated and actual latent positions, we apply a Procrustes transform [Gower, 1975] to the estimated latent positions $\hat{Z}$.

The root mean squared error (RMSE) for the latent positions, each of the model parameters, and baseline intensities μ_{uv} for all node pairs is shown in Figure B.1. As the time duration T increases, more events are generated. Notice that the errors are all decreasing with increasing T as one would expect.

B.2 REAL NETWORK DATASET DESCRIPTIONS

We perform experiments on several real network datasets:

- Reality mining dataset [Eagle and Pentland, 2006] is derived from the Reality Commons project from 14 September 2004 to 5 May 2005. The dataset we use contains 65 students and 2150 communications (Denote as Reality).
- Enron email dataset [Klimt and Yang, 2004] consists communications among 155 Enron individuals. It contains 9,646

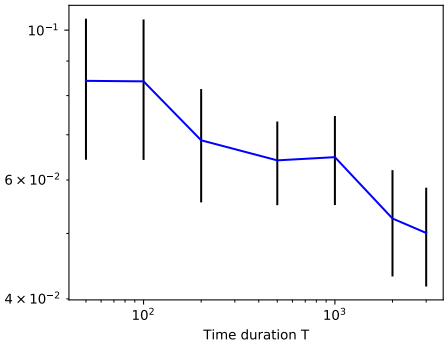

(a) latent positions z

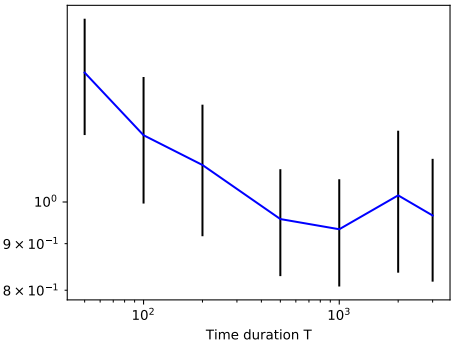

(b) sender effects δ

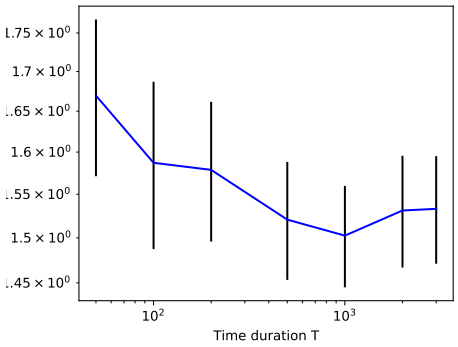

(c) receiver effects γ

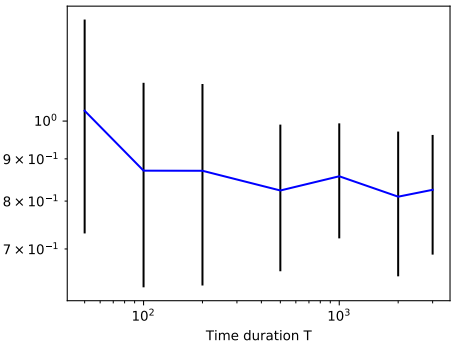

(d) intercept parameter θ_2

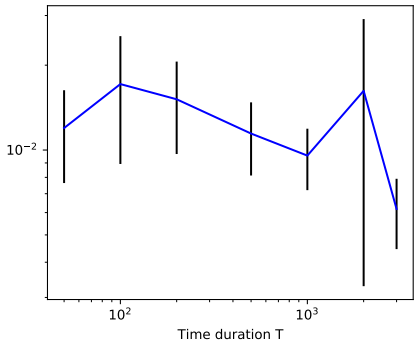

(e) jump size for self-exciting term α_1

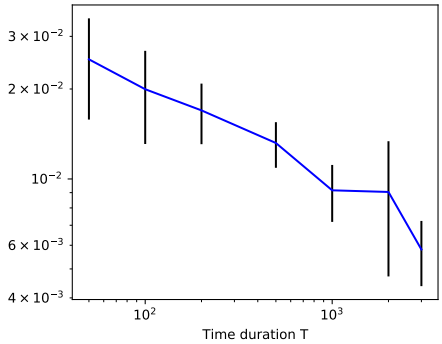

(f) jump size for reciprocal term α_2

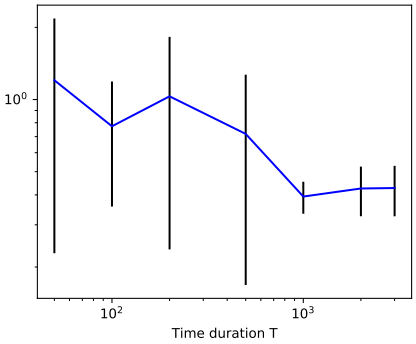

(g) baseline intensity μ

Figure B.1: Root mean square error over 30 simulated networks ($\pm$ 2 standard errors) for different parameters

email message spanning a period of 453 days. This dataset is tested in Yang's paper for their DLS model (Denote as Enron)

- The Militarized Interstate Disputes (MID) dataset [Palmer et al., 2021] consists of 145 countries with 5088 Disputes among them with a period of 8380 days (Denote as MID).
- Facebook-forum dataset [Rossi and Ahmed, 2015] consists of 899 students posted 33,720 broadcast messages in the forum over 165 days (Denote as FB-forum).

For the Reality, FB-forum, and MID datasets, we re-scale the timestamps so that they are in all $[0, 1000]$ in the same manner as Arastuie et al. [2020]. For Enron, we keep the same scale as Yang et al. [2017] to make a fair comparison against the DLS model.

B.3 DESCRIPTIONS OF OTHER MODELS

Dual Latent Space (DLS) Model We use the implementation at `https://github.com/jiaseny/lspp` for the DLS model. We provide a detailed comparison of the DLS model with our proposed LSH model in Section 3.2. It adopts a bivariate Hawkes process and latent space-based approach to capture homophily and reciprocity of continuous-time dynamic networks. Unlike our proposed LSH model, the DLS model does not have the self-excitation term. Their reciprocal terms are parameterized by multiple latent spaces associated with different decay values.

Hawkes Process-based Block Models We use the implementation at `https://github.com/IdeasLabUT/CHIP-Network-Model` for the Community Hawkes Independent Pairs (CHIP) model [Arastuie et al., 2020] and the Block Hawkes Model (BHM) [Junuthula et al., 2019]. CHIP is a univariate Hawkes process network model with block structure where each node pair is independent of all others. The BHM is also a univariate Hawkes process network model with block structure; however, an event between a node pair equally excites all node pairs in the same block pair.

Continuous-time Dynamic Network Embeddings (CTDNE) We used the same hyperparameters ($d = 128, R = 10, L = 80, \omega = 10$) as mentioned in Nguyen et al. [2018]. We used the implementation from the StellarGraph package [Data61, 2018]. We used timestamps up to t_i (beginning of test window) to create both temporal walks and the classifier's positive and negative examples. Edges feature vector is computed using weighted-L2 operation. To create walks, we test using directed/undirected graphs, also varied the neighbor selection distribution between biased(exponential)/unbiased. Best results are reported for each dataset.

B.4 DYNAMIC LINK PREDICTION

In section 5.2.1, we perform dynamic link prediction experiments. In this section, we demonstrate more results of the AUC values and the ROC curves over 100 time intervals for different models and different real world datasets.

Figure B.2 shows the boxplot of the AUC values for dynamic link prediction over 100 random time intervals. The DLS model does not scale to the fb-forum dataset. The box plot indicates that our proposed model achieves the best in MID and fb-forum dataset and is competitive in Reality and Enron datasets. Moreover, in the fb-forum, MID, and Enron datasets, the dispersion in AUC values from our model is less as evidenced by the low width of the boxes. In all datasets, the bulk of the distribution of AUC values for our LSH model is above 90% indicating a superior performance in the dynamic link prediction task.

Figure B.3-B.6 demonstrate the corresponding ROC curves for different models and real world datasets. The curves matches what we observed in Table 2 that our proposed model outperforms other models on MID and fb-forum and is competitive on Reality and Enron.

B.5 POSTERIOR PREDICTIVE CHECKS

As we discussed in Section 5.2.2, we simulate 15 networks from the fitted model and demonstrate the PPCs on the statistics in Table 3. We show the corresponding histogram of the PPCs for Reality Mining in Figures B.7 and B.8 for LSH and DLS, respectively. The actual value of the statistics is plotted as the blue vertical line. The red vertical line indicates the mean value of the statistics observed over the 15 simulated networks. Each figure consists of five subplots. The first, third, fourth, and fifth subplots give the histograms of average clustering coefficient, counts of events, reciprocity, and transitivity

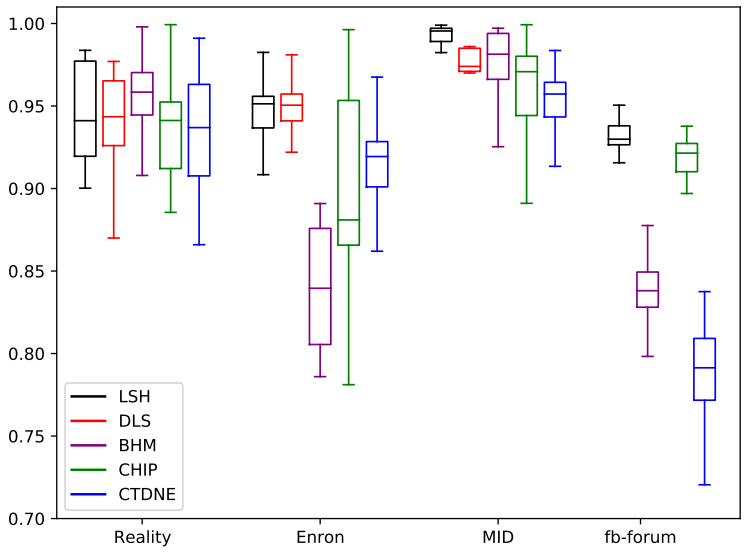

Figure B.2: AUC values for dynamic link prediction over 100 random time intervals

observed over the 15 simulated networks. The second subplot in each figure shows the histogram of the degree distribution. The left is the actual degree distribution, and the right is the degree distribution of the mean degree for each node of 15 simulated networks.

In general, the LSH performs quite well on generating average clustering coefficients, number of events, reciprocity, transitivity, and degree distribution that are similar to what is observed in the corresponding real dataset. The DLS performs well on the average clustering coefficients, the transitivity, and the degree distribution but simulates orders of magnitude more events. The DLS model also fails to simulate the high reciprocity observed in the data.

C ADDITIONAL CASE STUDY RESULTS

Figures C.1 and C.2 show zoomed in versions of the latent space for the positive slope model shown in Figures 2a and 3, respectively. In Table C.1, we show pairs of countries that have the top 50 number of incidents by one country towards another. In Figures 2 and C.1, we draw edges to represent the top 10 frequently occurring incidence between pairs of countries in Table C.1. The edges with two-way arrows indicate that they serve both as initiator and receiver to the other (e.g. PRK and ROK both have disputes with the other with the number of incidences 109 and 95, respectively).

Tables C.2 and C.3 show the estimated sender and receiver effects parameters from the LSH model with positive and negative slope, respectively. To compare with the highlighted countries in Figure 2 and C.1, countries that initiate more incidents tend to have higher sender effect and countries that receive more incidents tend to have higher receiver effect, e.g. USA has sender effect 4.18, and Yugoslavia (YUG) has receiver effect 3.03.

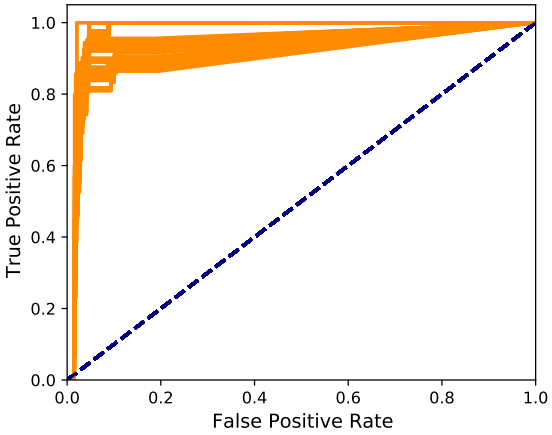

(a) ROC curve of LSH model for Reality Mining

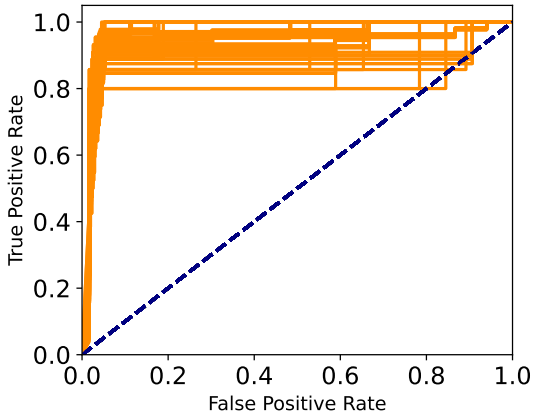

(b) ROC curve of DLS model for Reality Mining

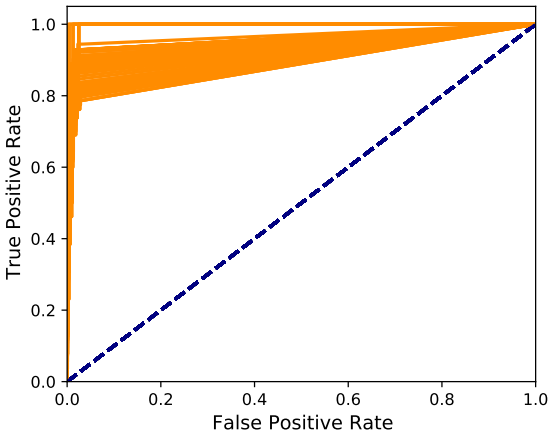

(c) ROC curve of CHIP model for Reality Mining

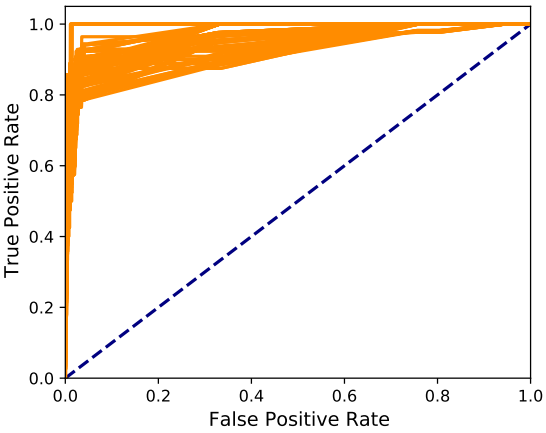

(d) ROC curve of BHM model for Reality Mining

Figure B.3: Dynamic link prediction on 100 random time intervals on Reality Mining

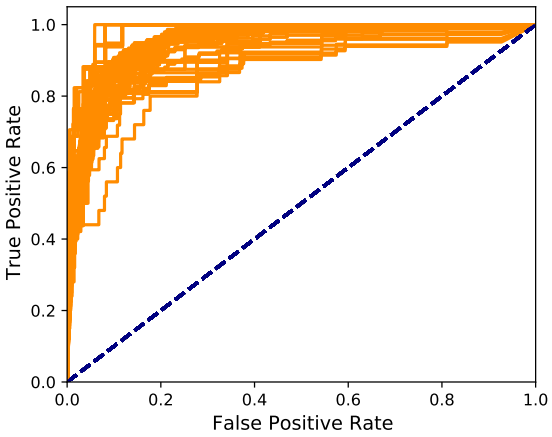

(a) ROC curve of LSH model for Enron

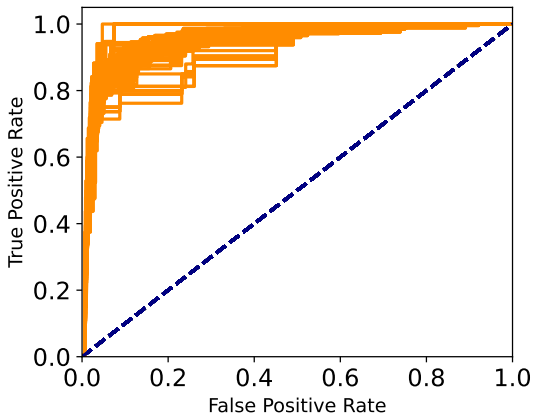

(b) ROC curve of DLS model for Enron

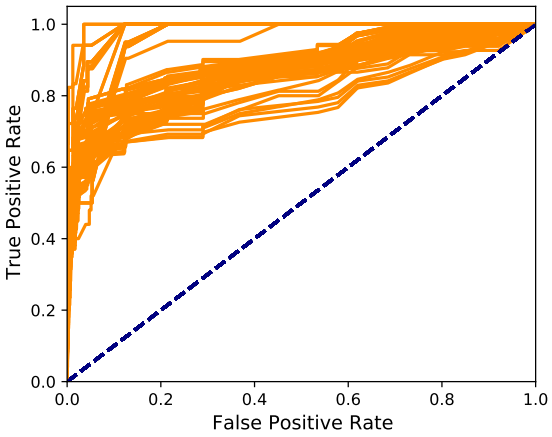

(c) ROC curve of CHIP model for Enron

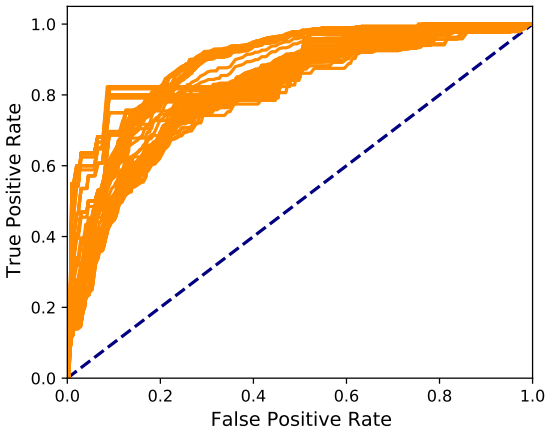

(d) ROC curve of BHM model for Enron

Figure B.4: Dynamic link prediction on 100 random time intervals on Enron

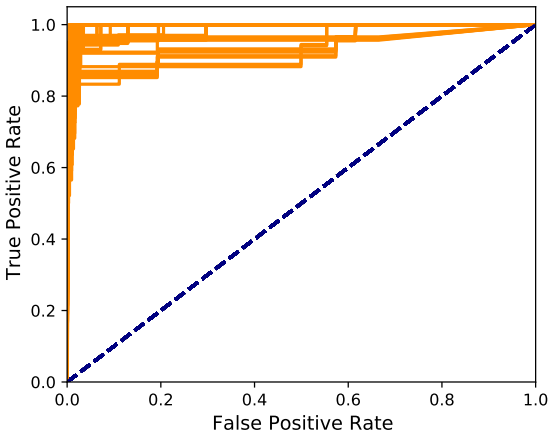

(a) ROC curve of LSH model for MID

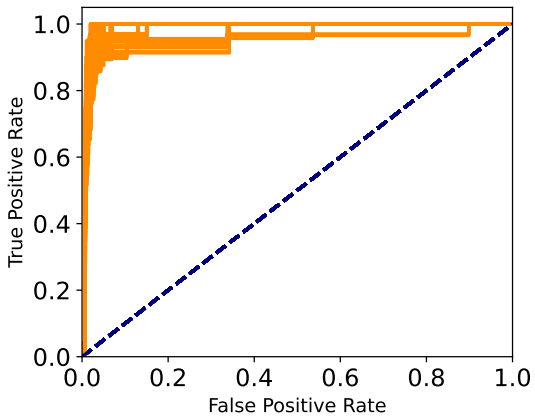

(b) ROC curve of DLS model for MID

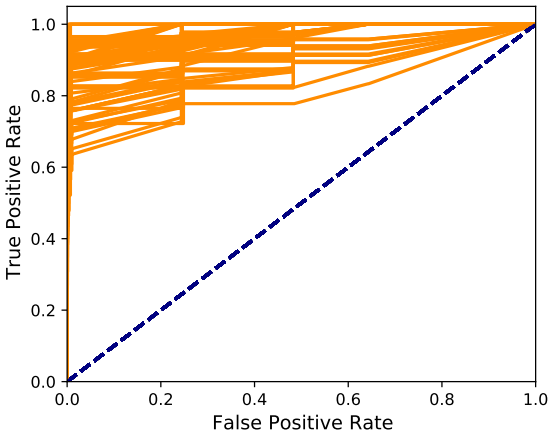

(c) ROC curve of CHIP model for MID

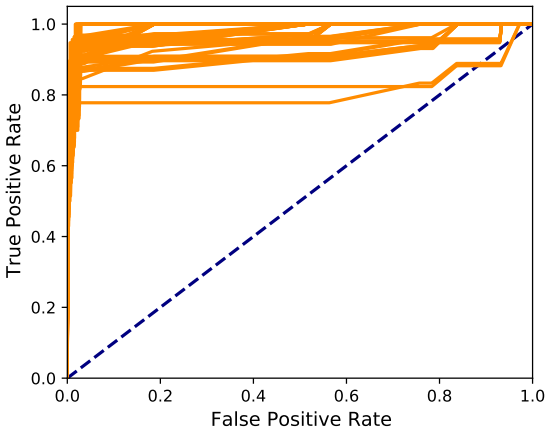

(d) ROC curve of BHM model for MID

Figure B.5: Dynamic link prediction on 100 random time intervals on MID

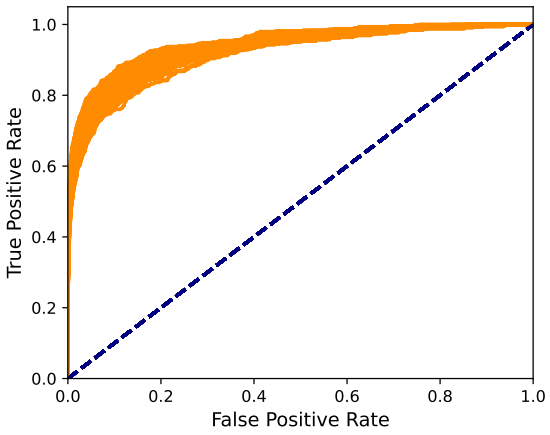

(a) ROC curve of LSH model for fb-forum

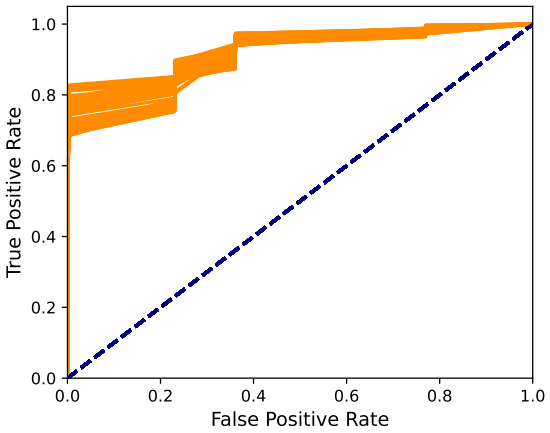

(b) ROC curve of CHIP model for fb-forum

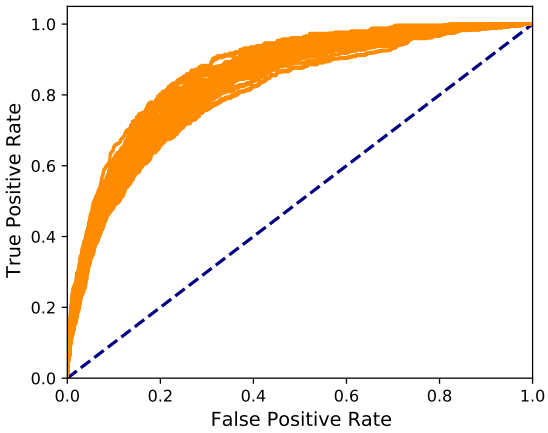

(c) ROC curve of BHM model for fb-forum

Figure B.6: Dynamic link prediction on 100 random time intervals on fb-forum

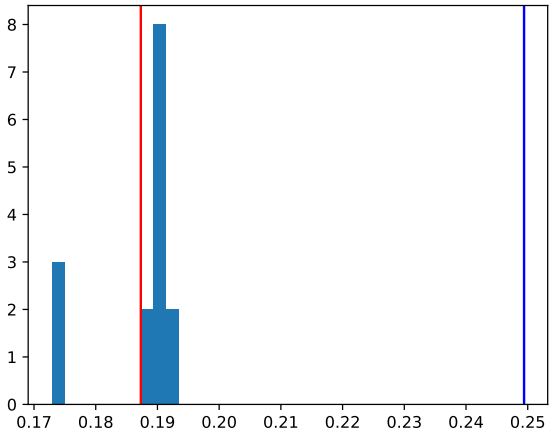

(a) Histogram of average clustering coefficients

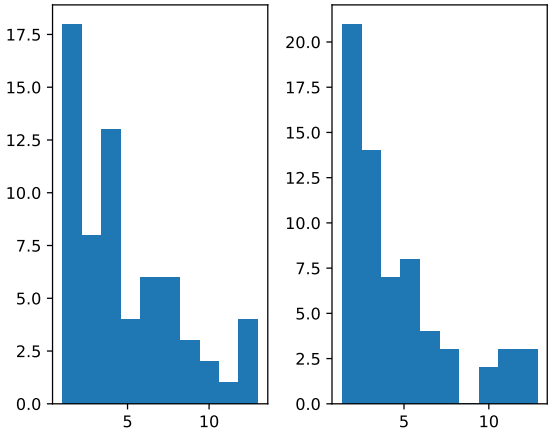

(b) Histogram of degree distribution for real network(left) and mean of 15 simulated networks (right)

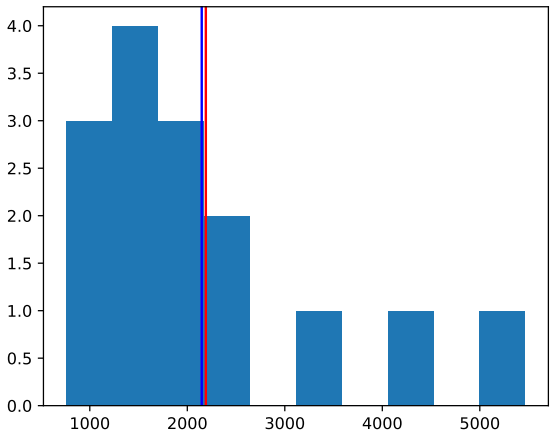

(c) Histogram of number of counts

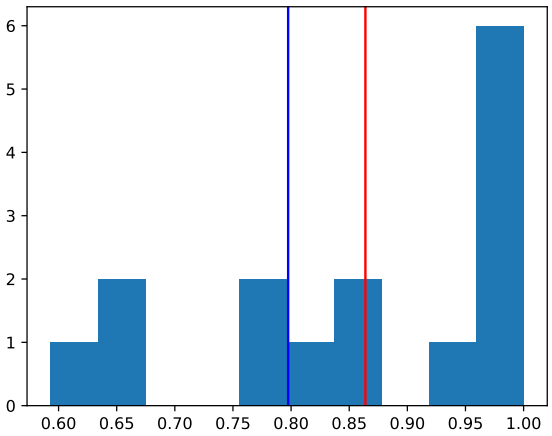

(d) Histogram of reciprocity

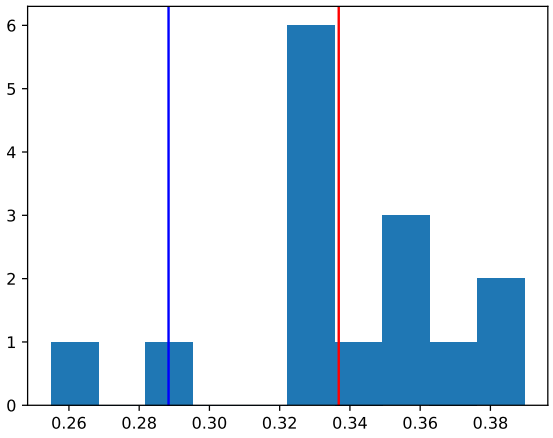

(e) Histogram of transitivity

Figure B.7: Histogram of 15 simulations from the LSH model fitted to Reality mining (blue line: actual value; red line: mean of 15 simulated values).

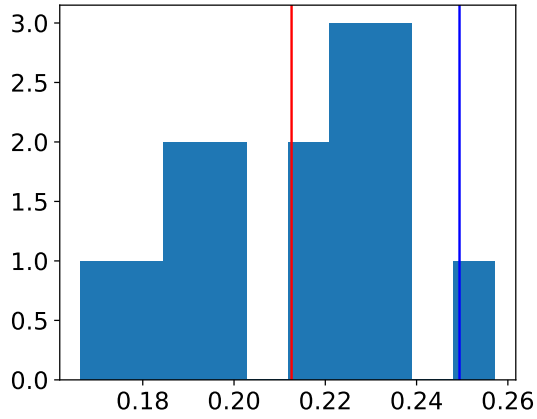

(a) Histogram of average clustering coefficients

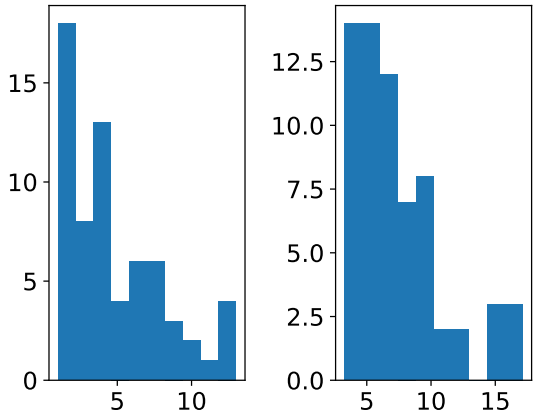

(b) Histogram of degree distribution for real network(left) and mean of 15 simulated networks (right)

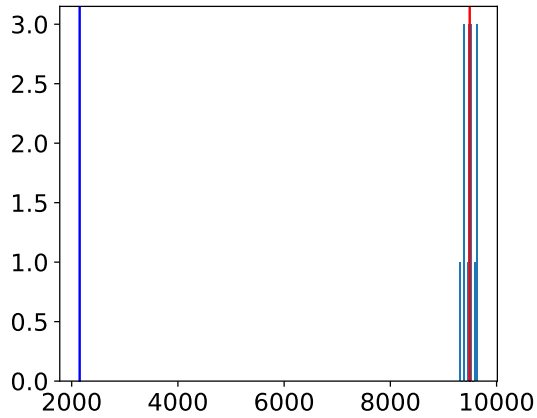

(c) Histogram of number of counts

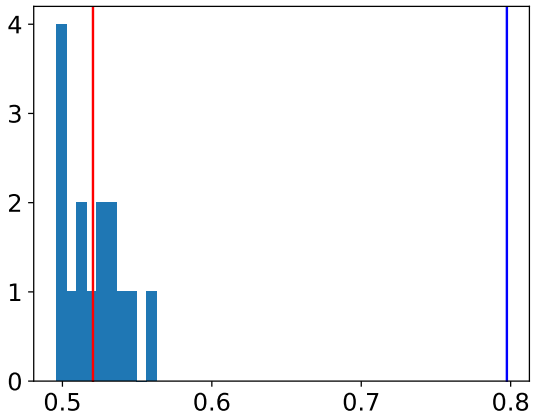

(d) Histogram of reciprocity

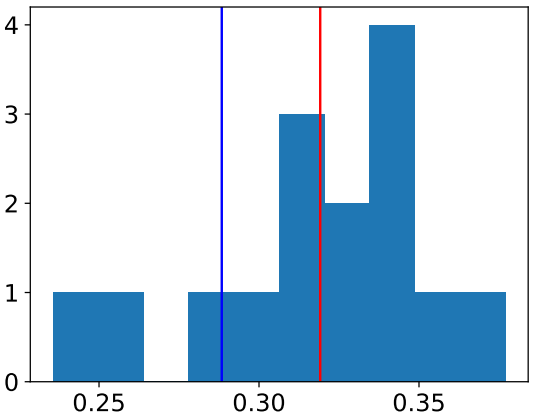

(e) Histogram of transitivity

Figure B.8: Histogram of 15 simulations from the DLS model fitted to Reality mining (blue line: actual value; red line: mean of 15 simulated values).

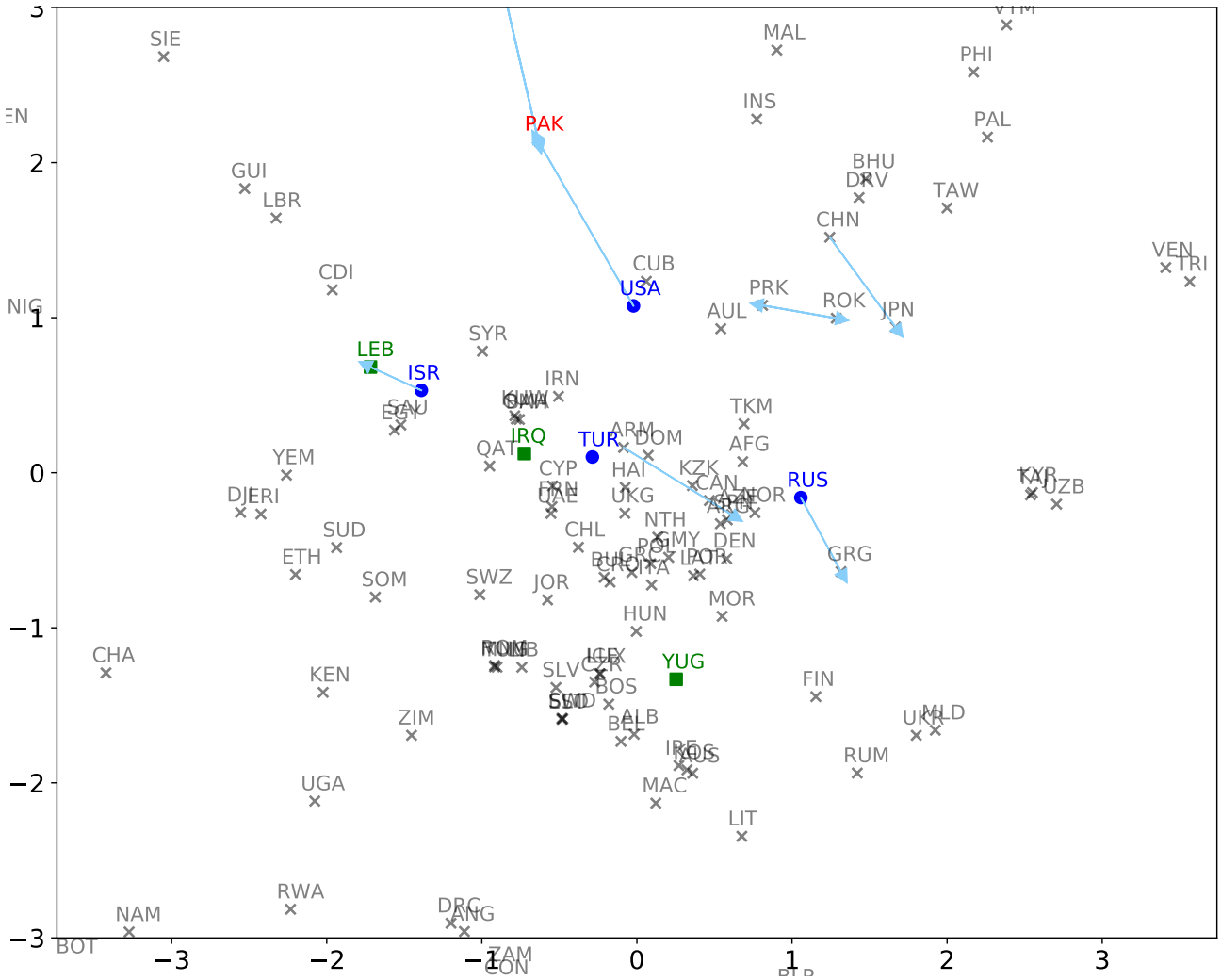

Figure C.1: 2-D latent space plot for MID data with positive slope (zoomed in version of Figure 2a).

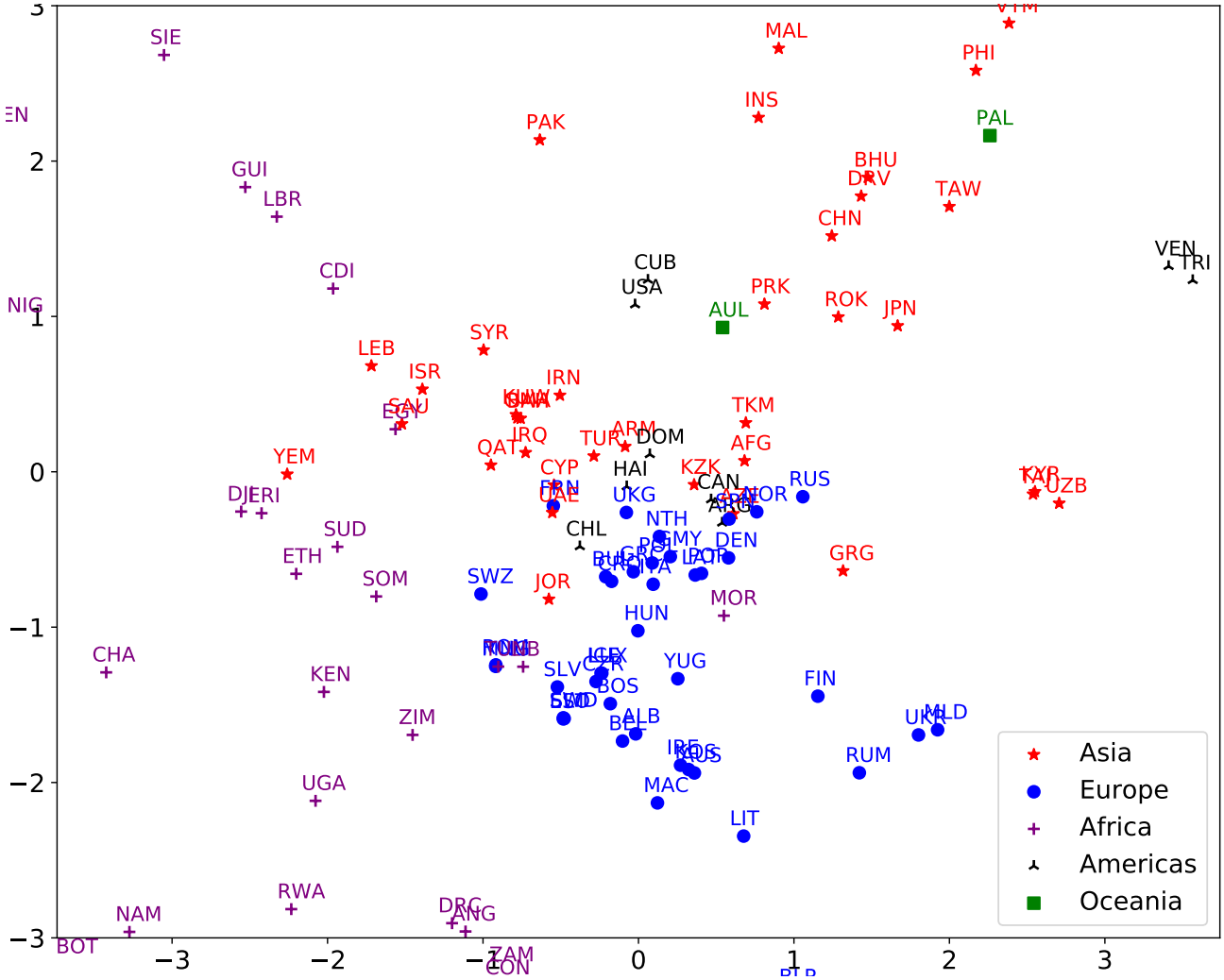

Figure C.2: 2-D latent space plot for MID data with positive slope and countries colored by continent (zoomed in version of Figure 3).

Table C.1: Pairs of countries that have the top 50 highest incidents

Initiator	Receiver	# of incidents	Initiator	Receiver	# of incidents
ISR	LEB	588	CHN	TAW	38
PAK	IND	174	YUG	ALB	37
USA	IRQ	174	SYR	TUR	34
USA	PAK	140	ALB	YUG	31
ARM	AZE	128	JPN	CHN	31
IND	PAK	116	USA	PRK	29
CHN	JPN	110	IRQ	USA	29
PRK	ROK	109	UKG	YUG	29
ROK	PRK	95	KUW	IRQ	28
RUS	GRG	88	LEB	ISR	28
TUR	GRC	85	FRN	YUG	27
UKG	IRQ	83	AZE	ARM	26
TUR	IRQ	80	RUS	JPN	26
GRC	TUR	73	PHI	CHN	26
SYR	LEB	61	NTH	YUG	26
PAK	AFG	61	ITA	YUG	26
TUR	SYR	54	CAM	THI	25
TUR	CYP	53	TAW	CHN	25
IRN	IRQ	53	SUD	UGA	25
THI	CAM	52	GMY	YUG	25
AFG	PAK	51	TUR	YUG	25
ISR	SYR	50	BEL	YUG	24
RUS	AFG	44	UKR	RUS	24
IND	BNG	44	GRG	RUS	24
USA	YUG	39	GRC	YUG	24

Table C.2: Nodal effect parameters estimated by the model with positive slope

Country	send	receive	Country	send	receive	Country	send	receive	Country	send	receive
AFG	-3.64	1.27	DRV	-1.30	-0.67	LUX	-0.40	-4.26	SPN	1.31	-0.85
ALB	0.34	-0.11	ECU	2.41	-1.91	MAA	-3.89	2.14	SRI	-0.08	-1.67
ALG	0.63	-1.72	EGY	0.78	0.14	MAC	-2.13	0.93	SUD	1.56	2.03
ANG	0.81	0.69	EQG	2.07	-2.21	MAL	0.89	-4.16	SUR	1.75	-0.94
ARG	0.50	-5.22	ERI	1.95	1.63	MLD	-0.49	1.51	SWD	-1.10	-0.62
ARM	-0.24	-1.25	EST	-1.10	-0.59	MLI	1.62	4.58	SWZ	-4.77	-0.10
AUL	1.59	-2.00	ETH	1.77	0.72	MNG	-1.01	-3.76	SYR	0.53	0.45
AUS	-4.54	-0.48	FIN	-4.57	0.24	MOR	-0.97	-1.71	TAJ	2.03	0.20
AZE	0.10	-0.44	FRN	1.44	-0.51	MYA	-3.80	5.48	TAW	1.62	1.35
BAH	-0.20	-5.32	GHA	3.34	2.57	NAM	0.95	1.69	TAZ	0.49	2.61
BEL	0.22	0.13	GMY	0.93	-1.88	NEP	-0.59	-1.87	THI	-0.71	5.22
BEN	-2.42	-0.74	GRC	1.04	-1.54	NIC	3.32	4.88	TKM	-0.29	-5.54
BHU	-4.13	-1.45	GRG	-4.07	1.20	NIG	5.07	0.91	TOG	2.51	1.24
BLR	1.53	-2.74	GUI	1.96	-0.64	NIR	0.28	1.65	TRI	-3.71	0.22
BNG	0.24	2.57	GUY	-2.08	1.76	NOR	1.17	-1.04	TUN	-1.01	-3.70
BOS	-5.06	-0.15	HAI	-4.64	0.10	NTH	1.28	-1.90	TUR	2.78	-0.15
BOT	0.36	-2.67	HON	1.45	5.06	OMA	-0.12	-5.26	UAE	0.69	-1.67
BRA	1.48	-0.80	HUN	0.35	-4.19	PAK	2.60	2.28	UGA	1.50	3.01
BUI	0.89	3.81	ICE	-0.41	-4.25	PAL	-0.81	-2.12	UKG	1.96	-1.84
BUL	-0.26	-0.92	IND	3.45	5.07	PER	-1.27	2.49	UKR	0.88	2.62
CAM	-3.86	6.68	INS	1.78	0.67	PHI	-0.57	2.52	USA	4.18	1.10
CAN	1.81	-1.28	IRE	-4.26	-0.67	PNG	-1.65	1.71	UZB	2.75	0.95
CAO	6.17	-0.29	IRN	2.67	0.91	POL	0.33	-1.41	VEN	2.45	1.92
CDI	1.28	0.85	IRQ	0.82	2.53	POR	0.60	-1.12	VTM	0.04	2.75
CEN	3.80	-4.27	ISR	2.19	-0.13	PRK	2.00	0.68	YEM	-3.84	0.63
CHA	2.67	2.92	ITA	0.63	-1.73	QAT	0.68	-4.92	YUG	2.78	3.03
CHL	-4.97	-1.65	JAM	1.47	-1.14	ROK	1.30	-0.10	ZAM	-1.12	1.43
CHN	3.76	1.53	JOR	-0.31	-1.25	ROM	-0.98	-3.77	ZIM	-0.33	0.32
COL	2.77	4.73	JPN	2.25	1.68	RUM	-3.02	1.13			
CON	-4.47	1.89	KEN	0.55	1.62	RUS	4.01	1.82			
COS	-1.90	0.12	KOS	-4.18	-0.56	RWA	0.62	3.04			
CRO	0.61	-0.45	KUW	0.17	-5.34	SAL	-4.19	2.05			
CUB	0.02	-5.59	KYR	2.01	0.08	SAU	0.56	-0.10			
CYP	-4.62	-1.33	KZK	0.20	-5.64	SIE	-1.30	2.40			
CZR	-0.44	-3.13	LAT	-0.83	-1.44	SIN	-4.26	1.08			
DEN	1.09	-1.59	LBR	1.94	1.34	SLO	-1.11	-0.60			
DJI	-1.61	0.25	LEB	-3.94	-0.30	SLV	-1.14	-0.11			
DOM	-0.35	-5.66	LIB	0.30	2.93	SOL	-4.57	3.22			
DRC	1.50	3.37	LIT	0.56	1.77	SOM	-4.16	1.04			

Table C.3: Nodal effect parameters estimated by the model with negative slope

Country	send	receive	Country	send	receive	Country	send	receive	Country	send	receive
AFG	-1.49	3.09	DRV	-1.50	-0.16	LUX	0.43	-1.59	SPN	1.58	1.20
ALB	1.12	-0.16	ECU	0.27	-2.38	MAA	-1.55	-0.37	SRI	-0.51	-1.48
ALG	-0.49	-2.00	EGY	0.43	0.44	MAC	-1.34	0.65	SUD	1.37	1.89
ANG	1.42	-0.42	EQG	-0.41	-1.40	MAL	0.80	-1.39	SUR	-0.44	-1.67
ARG	1.07	-1.38	ERI	1.11	-0.54	MLD	-0.79	-0.25	SWD	-0.52	-0.38
ARM	-0.28	0.59	EST	-0.45	-0.53	MLI	-0.41	0.46	SWZ	-1.55	0.51
AUL	1.39	-0.28	ETH	0.88	-0.25	MNG	-0.66	-1.42	SYR	0.34	0.95
AUS	-1.74	-0.30	FIN	-1.69	0.43	MOR	-0.36	-0.54	TAJ	0.55	-0.41
AZE	0.02	1.38	FRN	1.94	0.98	MYA	-1.53	1.08	TAW	0.59	0.67
BAH	-0.37	-1.60	GHA	0.43	-1.40	NAM	0.46	-0.27	TAZ	-0.38	-1.69
BEL	0.76	0.61	GMY	1.38	-0.26	NEP	-0.42	-1.39	THI	0.14	0.91
BEN	-1.63	-0.32	GRC	1.59	-0.21	NIC	0.46	-0.22	TKM	-0.36	-1.41
BHU	-1.49	-0.37	GRG	-1.62	1.36	NIG	1.34	-0.86	TOG	-1.56	-0.41
BLR	-0.52	-1.40	GUI	0.82	-1.57	NIR	-0.55	-0.42	TRI	-2.01	-0.30
BNG	0.49	-1.80	GUY	-1.50	0.54	NOR	0.98	0.17	TUN	-0.41	-1.53
BOS	-1.48	0.48	HAI	-1.55	1.85	NTH	1.64	-0.24	TUR	2.60	1.34
BOT	-0.51	-1.45	HON	-0.51	0.37	OMA	-0.21	-1.41	UAE	1.15	-0.45
BRA	-0.49	-1.66	HUN	1.29	-1.28	PAK	0.47	0.71	UGA	0.48	1.64
BUI	-0.37	0.54	ICE	0.50	-1.37	PAL	-0.37	-1.62	UKG	2.18	-0.29
BUL	0.46	0.36	IND	-0.26	1.43	PER	-1.56	0.17	UKR	-0.37	1.27
CAM	-1.75	0.54	INS	1.26	1.25	PHI	-0.36	1.51	USA	3.04	1.74
CAN	2.13	0.60	IRE	-1.66	-0.29	PNG	-0.36	-0.32	UZB	0.95	-1.35
CAO	-0.45	-0.75	IRN	1.78	2.12	POL	0.92	-0.23	VEN	0.93	-0.19
CDI	0.50	1.25	IRQ	-0.17	3.36	POR	1.06	0.62	VTM	0.30	0.99
CEN	0.30	-1.38	ISR	2.00	-0.26	PRK	0.59	1.69	YEM	-1.48	0.57
CHA	1.13	1.30	ITA	1.19	-0.41	QAT	1.23	-1.36	YUG	3.05	3.66
CHL	-1.49	-0.26	JAM	-0.53	-1.68	ROK	0.47	0.75	ZAM	-1.48	0.45
CHN	2.81	1.04	JOR	0.35	-0.26	ROM	-0.36	-1.85	ZIM	0.56	-0.45
COL	-1.44	0.86	JPN	-0.38	1.60	RUM	-1.29	0.50			
CON	-1.94	0.61	KEN	0.35	-0.26	RUS	3.40	2.59			
COS	-0.39	-1.42	KOS	-1.49	-0.45	RWA	-0.38	1.63			
CRO	1.27	0.96	KUW	-0.29	-1.38	SAL	-1.72	-0.53			
CUB	-0.50	-1.44	KYR	-1.27	0.56	SAU	0.49	0.56			
CYP	-1.55	-0.22	KZK	0.36	-1.71	SIE	-1.64	1.18			
CZR	0.32	-1.29	LAT	-0.54	-0.22	SIN	-1.55	-0.29			
DEN	1.39	-0.11	LBR	0.30	1.02	SLO	-0.51	-0.38			
DJI	-1.62	-0.38	LEB	-1.50	-0.59	SLV	-0.43	0.49			
DOM	-0.28	-1.72	LIB	0.55	3.34	SOL	-1.51	-0.34			
DRC	1.58	0.75	LIT	0.49	1.08	SOM	-1.49	1.05			